2021 43rd Annual International Conference of the
IEEE Engineering in Medicine & Biology Society (EMBC)
Oct 31 - Nov 4, 2021. Virtual Conference

Novel 3D-printed Electrodes for Implantable Biopotential Monitoring

Parvez Ahmmed[1], *Student Member, IEEE*, James Reynolds[1], *Student Member, IEEE*,
Shu Hamada[2], Prafulla Regmi[3], and Alper Bozkurt[1], *Senior Member, IEEE*

***Abstract*— A major bottleneck in the manufacturing process of a medical implant capable of biopotential measurements is the design and assembly of a conductive electrode interface. This paper presents the use of a novel 3D-printing process to integrate conductive metal surfaces on a low-temperature co-fired ceramic base to be deployed as electrodes for electrocardiography (ECG) implants for small animals. In order to fit the ECG sensing system within the size of an injectable microchip implant, the electronics along with a pin-type lithium-ion battery are inserted into a cylindrical glass tube with both ends sealed by these 3D printed composite electrode discs using biomedical epoxy. In the scope of this paper, we present a proof-of-concept *in vivo* experiment for recording ECG from an avian animal model under local anesthesia to verify the electrode performance. Simultaneous recording with a commercial device validated the measurements, demonstrating promising accuracy in heart rate and breathing rate monitoring. This novel technology could open avenues for the mass manufacturing of miniaturized ECG implants.**

***Clinical relevance*— A novel manufacturing process and an implantable system are presented for continuous physiological monitoring of animals to be used by veterinarians, animal scientists, and biomedical researchers with potential future applications in human health monitoring.**

I. Introduction

Continuous and wireless physiological monitoring would enable veterinarians, animal scientists, and biomedical researchers to better understand and monitor animal health and welfare [1]. Traditional methods of animal health monitoring devices, especially for small animals, require benchtop instrumentation connected to the animals by wires and are only suitable for clinical settings. Moreover, external attachment of biopotential electrodes requires hair removal and adhesives, which make the animals uncomfortable with the devices during long-term use [2]. A subcutaneously injected sensor (Fig. 1), on the other hand, allows for free movement of animals and hence offers deeper insight into their physiological status in natural or semi-natural settings.

Electrocardiography (ECG) can provide some of the most important physiological endpoints that can be used to assess the animal's health and welfare status: heart rate (HR), heart rate variability (HRV), and potentially breathing rate (BR). However, it is challenging to manufacture the miniaturized electrodes needed to successfully integrate ECG recording circuitry into an implantable form factor [3], [4], [5]. The electrodes need a consistent low-impedance connection from the tissue to the circuit, while the electronics in the implant need to be completely insulated from the outside environment. This low-impedance connection requires the protrusion of conductors out of the implant packaging and a larger surface area of electrode contact with the tissue. Scalability and lower cost of the electrode manufacturing process are also necessary for commercial applications.

Existing electrode designs in the literature use either a spiraled wire [3] or micromachined metal [4], [5] as the conductor. Some of the primary drawbacks of these methods include the requirement for manual production by hand, a difficult manufacturing process, increased cost, and the lack of uniformity of the end product.

Our initial attempt of designing a subcutaneous electrophysiology implant for monitoring HR used stainless steel wires as electrodes [6]. Although the results were promising, the measurements were suboptimal due to the limited tissue-electrode contact and small spacing between the electrodes. Later, we investigated electrodes made of conductive epoxy, which showed performance comparable to the other metallic alternatives [7]. These epoxy electrodes provided more flexibility in terms of implant packaging and encapsulation. However, it involves trade-offs in size, uniformity, and manufacturing complexity compared with the electrodes presented in this paper.

In order to advance the mass production of lower-cost biopotential electrodes, additive manufacturing (i.e., 3D-printing) technology can play a significant role. In this work,

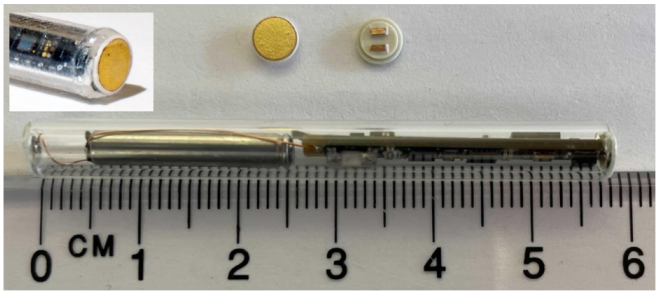

Fig. 1. Picture of the fully assembled implant with the electronics and the battery inserted into a glass tube. The two ends of the glass tube are sealed with two custom NeuroStone™ electrodes, laid out above the implant. The inset shows a close-up of one of the edges with the sealed electrode.

This work is supported by the National Science Foundation (NSF) through Grants CCSS-1554367 and ECC-1160483 (NERC for ASSIST).

[1]P. Ahmmed, J. Reynolds, and A. Bozkurt are with the Department of Electrical and Computer Engineering, NC State University, Raleigh, NC 27695-7911, USA (corresponding e-mail: aybozkur@ncsu.edu).

[2]S. Hamada is with Murata Manufacturing Co., Ltd., Kyoto 617-8555, Japan.

[3]P. Regmi was with the Prestage Department of Poultry Science, NC State University, Raleigh, NC 27695-7911, USA. He is now with the Department of Poultry Science, University of Georgia, Athens, GA 30602, USA.

NC State University, Raleigh, NC, USA collaborated with the Murata Manufacturing Co., Ltd., Kyoto, Japan, to explore the possible adoption of a novel technique for printing metal contacts on a co-fired ceramic base called Neurostone™ [8]. This novel technology allowed us to print the electrodes in bulk and to easily connect the external tissue surfaces to the electrophysiology front-end circuit inside the implant through the designed via links. Our use of these circular electrodes as end-caps for the cylindrical glass tubes (Fig. 1) helped us to encapsulate the implant electronics. In this work, we performed a proof-of-concept *in vivo* validation of this implant using a locally-anesthetized chicken subject and present our evaluation results in comparison with a commercial ECG monitoring device.

II. System Overview

This section gives an overview of the target application, which is a subcutaneous electrophysiology implant, and describes the implant packaging along with the design and construction of the proposed electrodes.

A. Implant Electronics

In order to provide the veterinarians and animal scientists a tool to assess the health and behavior of animals, we previously presented an implant with optical and motion-sensing capabilities which can be injected subcutaneously [9]. In the present work, we have included additional circuitry to enable the study of subcutaneous ECG in this form factor.

The relevant parts of the system, as shown in Fig. 2, include an analog front-end (AFE) for measuring ECG-based heart rate (MAX30003, 2.9 × 2.7 × 0.6 mm^3, Maxim Integrated, San Jose, CA, USA), a system-on-a-chip combining a microcontroller with a radio transceiver (CC2640, 2.7 × 2.7 × 0.5 mm^3, Texas Instruments, Dallas, TX, USA), and an integrated RF antenna (2450AT, 5.0 × 2.0 × 1.5 mm^3, Johanson Technology, Inc., Camarillo, CA, USA) designed for 2.4 GHz radio. A printed circuit board (PCB) with a width of 3.6 mm contains all the electronics and the contact pads for connecting the ECG electrodes and a 15-mAh Li-ion pin-type battery with a diameter of 3.6 mm (CG-320B, Panasonic Corporation, Kadoma, Osaka, Japan).

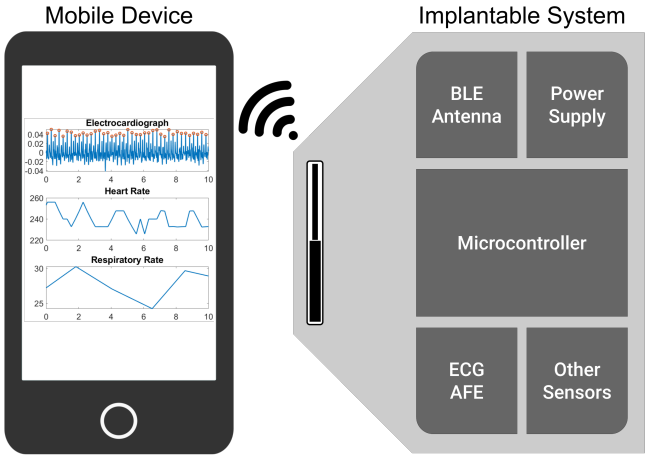

Fig. 2. Block diagram of the wireless electrophysiology monitoring system.

The integrated circuit MAX30003 is connected to the two electrode pads on the PCB through a network of passive components working as a filter. The AFE, then, processes the biopotential signal and sends the digitized data to the microcontroller through the SPI bus. The CC2640 is equipped with a Bluetooth™ Low Energy (BLE) radio for wireless communication. When a BLE host device establishes a connection with the implant, it transmits the collected data to the external data aggregator in real-time and consumes 0.77 mW power (expected battery life of ∽70 hours).

B. Implant Packaging

The PCB along with the soldered components is first coated with a biomedical epoxy (M-31CL, Henkel Corporation, Düsseldorf, Germany) to seal all the electronics. The overall system, along with the soldered battery, securely fits into a borosilicate glass cylinder with an inner diameter of 4 mm. The two electrodes in the shape of circular discs are used as lids for the glass tube (Fig. 1).

There are two main constraints on the electrode design imposed by this application: 1) the size of the circular base needs to be larger than the inner diameter of the glass tube, and 2) a through-hole via needs to connect the outer electrode surface to the inner soldering pad (Fig. 3). Murata's NeuroStone™ technology makes such a design possible by combining a multi-material 3D-printing process with custom inks for ceramic, copper, and support materials [8].

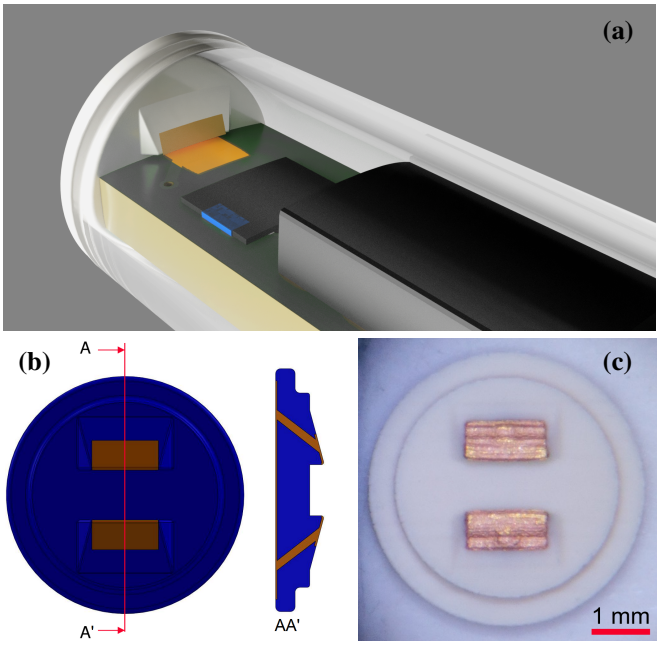

Fig. 3. (a) Detailed illustration showing the attachment of the NeuroStone™ electrode to the PCB. (b) CAD design of the electrode illustrating the metallic via for connecting the two sides and the grove for inserting the PCB in the cross-sectional view. (c) Picture of a printed electrode highlighting the solder pads on the inner side of the ceramic base and the circular grove for fitting to the glass tube.

C. Electrode Design and Construction

Designed using a commercial CAD tool (3D-CAD, Autodesk, Inc., San Rafael, CA, USA), the electrode discs have an outer diameter of 5 mm. The outer side of the disc has a large electrode surface while the inner side has two symmetrical soldering pads separated by a 1-mm groove for the PCB (Fig. 3). This helps the disc to be placed at one end of the PCB and soldered to the PCB pad. The inner side of the disc also has a circular groove to help center the electrode within the glass tube.

Manufacturing the electrode begins with converting the design files to use with the inkjet printer. The deposition process involves the inkjet print-heads simultaneously layering inks containing low-temperature co-fired ceramic (LTCC), copper, and a support material on a heated platform. These layers harden as the solvents evaporate. After the layering of materials is complete, the electrode is placed in a hypoxic environment containing N_2/H_2 atmosphere and heated to above 800°C [8]. This co-firing process removes the support material, resulting in the presented electrode structure (Fig. 3). Finally, the surface of the copper electrode is coated with electroless nickel immersion gold (ENIG).

III. Experimental Results and Discussion

To validate the accuracy of our implant in estimating the HR and BR, we ran a proof-of-concept *in vivo* experiment with a 22-week old White Leghorn chicken (*Gallus gallus domesticus*) subject (Fig. 4). For comparison, we collected simultaneous ECG data using needle electrodes connected to a commercial device (Go Direct™ EKG Sensor, Vernier Software & Technology, Beaverton, OR, USA). All animal procedures were approved by the Institutional Animal Care and Use Committee (IACUC) of NC State University, Raleigh, NC, USA.

During this experiment, we applied local anesthesia to the dorsal side of the chicken and removed a few feathers to prepare the site of implantation. Then, we inserted the implant subcutaneously at the nape of the neck between the shoulder blades and established a wireless data connection between the implant and a remote laptop computer. To record ECG signals from both the devices simultaneously, we also attached three needle electrodes subdermally (two needles inserted adjacent to the implant and the third one in the right leg) for the Vernier device, which was connected to a computer through a USB cable (Fig. 4).

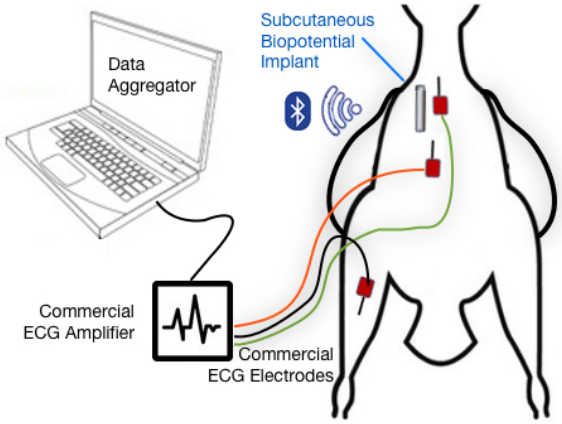

Fig. 4. Schematic diagram showing the *in vivo* experimental setup with a locally-anesthetized chicken for validating our system by comparing the measurements with a wired commercial ECG amplifier system.

Fig. 5 shows the raw ECG signals modulated by respiratory artifacts (baseline wander as defined in [10]) recorded from both the devices with a sampling frequency of 128 Hz. We used a 15-point moving average filter to extract the respiratory baselines. Once the baselines are subtracted from the raw ECG, we obtained the clean ECG signals (Fig. 6) which clearly coincided with each other. Finally, we performed peak detection using a library function *findpeaks* in MATLAB™ (Mathworks, Natick, MA, USA) on the filtered ECG signals and the ECG baselines, which are 3-minutes long, to get the R-R and respiratory intervals, respectively (Fig. 7).

Heart rate in beats per minute (BPM) and breathing rate in breaths per minute (BrPM) were calculated from these peak-to-peak intervals. The mean absolute percentage error and the Pearson correlation coefficient between the HR values from the two devices are 1.72% and 0.77 while those between the BR values are found to be 4.38% and 0.79, respectively. These as well as the other statistics calculated from these rates (Table I) demonstrate the ability of our implant to provide accurate physiological information.

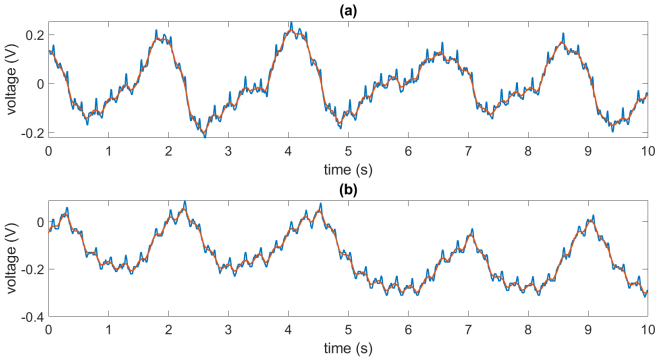

Fig. 5. Raw ECG data along with respiratory artifacts from (a) our implant and (b) Go Direct™. The red line represents the baseline for respiratory modulation.

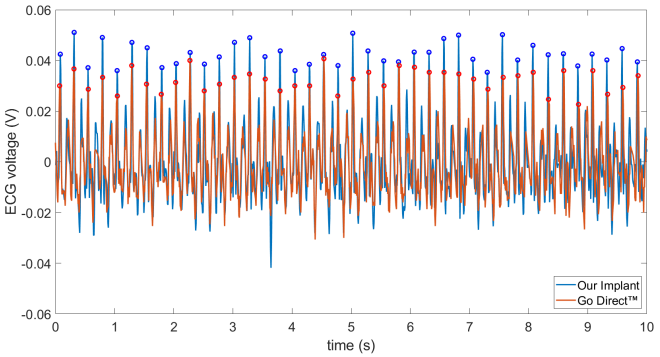

Fig. 6. Filtered ECG signals from both of the devices after subtracting the respiratory artifacts. The R-peaks of the cardiac cycles are circled.

We also observed a periodic modulation in heartbeat intervals (or heart rate) linked with respiratory artifacts (Fig. 7a), which is known as respiratory sinus arrhythmia (RSA). This physiological phenomenon, which causes the R-R interval to shorten during inhalation and lengthen during exhalation, is common in humans (especially neonates) and other vertebrates [11], [12]. To verify the effect of RSA on the R-R intervals, we applied a Discrete Fourier Transform (DFT) to the transient signals of R-R interval values and the respiratory baseline of the ECG waveform collected from the implant. Both signals showed peaks at the same frequency corresponding to the BR (Fig. 8). This reinforces the functionality of our implant in capturing useful physiological insight.

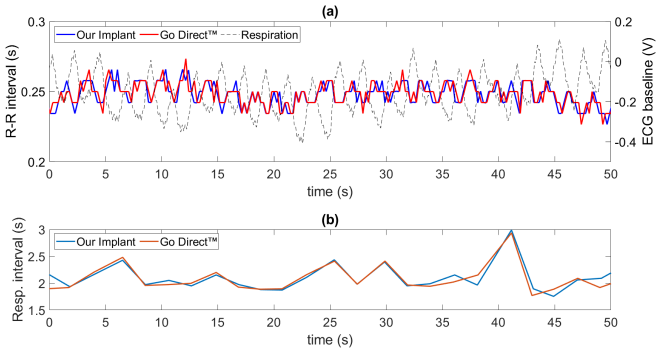

Fig. 7. (a) R-R intervals extracted using the clean ECG signals from both the devices. The respiratory baseline is also superimposed on the plot to demonstrate the effect of respiratory sinus arrhythmia. (b) Respiratory intervals calculated from the gap between consecutive peaks in the ECG baseline.

TABLE I
STATISTICAL COMPARISON BETWEEN THE DEVICES

Quantity (unit)		Presented Implant	Go Direct™
Heart rate (BPM)	Mean	244.64	244.20
	SD	8.87	9.03
Breathing rate (BrPM)	Mean	28.71	28.70
	SD	2.61	2.67

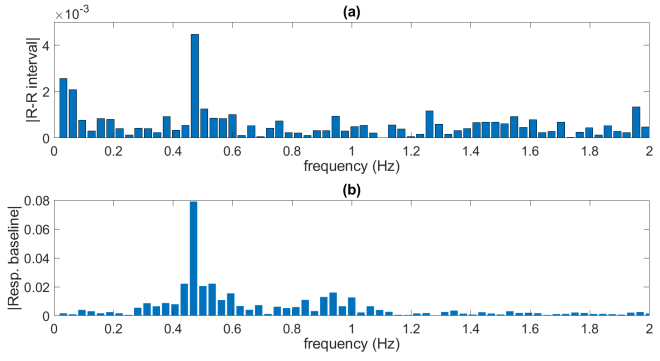

Fig. 8. Magnitude of DFT applied on (a) the R-R interval values, and (b) the respiratory baseline from the implantable device. The synchronized peak at approximately 0.47 Hz (28.2 BrPM) confirms the effect of respiratory sinus arrhythmia.

IV. CONCLUSION

A subcutaneously implantable biopotential sensor system has been developed to record continuous ECG for extracting heart rate and breathing rate in animals. The design and manufacturing of such implants had been hindered by the difficulties involved with biopotential electrode interfacing and its integration into miniaturized packaging. In order to facilitate the mass production of biopotential electrodes for this implant, the successful incorporation of a novel 3D-printing technology, NeuroStone™, is demonstrated. Proof-of-concept *in vivo* experimentation with a locally-anesthetized chicken produced promising results with an accuracy comparable to that of a commercial and benchtop ECG system. The presented subcutaneous implant device utilizing a novel electrode manufacturing technique can be a useful tool for animal scientists, veterinarians, and biomedical researchers for monitoring the physiology continuously in real-time and with a high resolution.

REFERENCES

[1] A. Jukan, X. Masip-Bruin, and N. Amla, "Smart computing and sensing technologies for animal welfare: A systematic review," *ACM Computing Surveys (CSUR)*, vol. 50, no. 1, pp. 1–27, Apr. 2017, Article no. 10.

[2] R. Brugarolas, T. Latif, J. Dieffenderfer, K. Walker, S. Yuschak, B. L. Sherman, D. L. Roberts, and A. Bozkurt, "Wearable heart rate sensor systems for wireless canine health monitoring," *IEEE Sensors Journal*, vol. 16, no. 10, pp. 3454–3464, May 2016.

[3] T. Volk, S. Gorbey, M. Bhattacharyya, W. Gruenwald, B. Lemmer, L. M. Reindl, T. Stieglitz, and D. Jansen, "RFID technology for continuous monitoring of physiological signals in small animals," *IEEE Transactions on Biomedical Engineering (TBME)*, vol. 62, no. 2, pp. 618–626, Feb. 2015.

[4] Á. Bjarnason, T. Vuorela, J. Verho, J. Riistama, J. Vanhala, J. Lekkala, and J. Hyttinen, "Implantable measurement system for dairy-cattle monitoring with long recording time," *Advances in Science and Technology*, vol. 85, pp. 33–38, Sept. 2012.

[5] J.-H. Lee and D.-W. Seo, "Development of ECG monitoring system and implantable device with wireless charging," *Micromachines*, vol. 10, no. 1, p. 38, Jan. 2019.

[6] J. M. Valero-Sarmiento, J. Reynolds, A. Krystal, and A. Bozkurt, "*In Vitro* evaluation of an injectable EEG/ECG sensor for wireless monitoring of hibernation in endangered animal species," *IEEE Sensors Journal*, vol. 18, no. 2, pp. 798–808, Jan. 2018.

[7] J. Reynolds, J. M. Valero-Sarmiento, J. Dieffenderfer, and A. Bozkurt, "The viability of conductive medical epoxy as an implantable electrode material," in *IEEE SENSORS*, Oct. 2017, pp. 1–3.

[8] T. Hirao and S. Hamada, "Novel multi-material 3-dimensional low-temperature co-fired ceramic base," *IEEE Access*, vol. 7, pp. 12 959–12 963, Jan. 2019.

[9] J. Reynolds, P. Ahmmed, and A. Bozkurt, "An injectable system for subcutaneous photoplethysmography, accelerometry, and thermometry in animals," *IEEE Transactions on Biomedical Circuits and Systems (TBCAS)*, vol. 13, no. 5, pp. 825–834, Oct. 2019.

[10] P. H. Charlton, D. A. Birrenkott, T. Bonnici, M. A. F. Pimentel, A. E. W. Johnson, J. Alastruey, L. Tarassenko, P. J. Watkinson, R. Beale, and D. A. Clifton, "Breathing rate estimation from the electrocardiogram and photoplethysmogram: A review," *IEEE Reviews in Biomedical Engineering*, vol. 11, pp. 2–20, Oct. 2018.

[11] J. Hayano, F. Yasuma, A. Okada, S. Mukai, and T. Fujinami, "Respiratory sinus arrhythmia: A phenomenon improving pulmonary gas exchange and circulatory efficiency," *Circulation*, vol. 94, no. 4, pp. 842–847, Aug. 1996.

[12] E. W. Taylor, D. Jordan, and J. H. Coote, "Central control of the cardiovascular and respiratory systems and their interactions in vertebrates," *Physiological reviews*, vol. 79, no. 3, pp. 855–916, July 1999.